Incident Angle Effect of Energetic Carbon Ions on Thickness, Morphology, and Structure of Ultrathin Amorphous Carbon Films Deposited by Filtered Cathodic Vacuum Arc

N. Wang and K. Komvopoulos

Department of Mechanical Engineering, University of California, Berkeley, California, 94720, USA

Abstract

In oblique deposition, the microstructure and film properties are strongly dependent on ion depositing and self-sputtering. The effect of the incident angle of energetic carbon ions on the deposition of ultrathin amorphous carbon (*a*-C) films by filtered cathodic vacuum arc (FCVA) was examined in the context of numerical and experimental results. The thickness of *a*-C films deposited at different incident angles was investigated in the light of Monte Carlo simulations, and the calculated depth profiles were compared with those obtained from high-resolution transmission electron microscopy (TEM). The surface morphology and structure of the *a*-C films were studied by atomic force microscopy (AFM) and X-ray photoelectron spectroscopy (XPS), respectively. The film thickness decreased with increasing incident angle, while the surface roughness increased and the content of tetrahedral carbon hybridization (sp^3) decreased significantly for incident angles above 45° measured from the surface normal. TEM, AFM, and XPS results indicate that the smoothest and thinnest *a*-C films with the highest content of sp^3 carbon bonding were produced for an incident angle of 45°. The findings of this study have direct implication in ultra-high-density magnetic recording, where ultrathin/smooth *a*-C films of high sp^3 content are of critical importance.

Index Terms – Amorphous carbon, hybridization, filtered cathodic vacuum arc, structure, surface morphology, ultrathin films.

Submitted to *IEEE Transactions on Magnetics*.

I. Introduction

Amorphous carbon (*a*-C) films are widely used as protective overcoats mainly due to their high hardness and good wear resistance [1–3]. An application where *a*-C films are of paramount importance to device reliability and performance is hard-disk drives (HDDs). In HDDs, information is stored in the magnetic medium of a hard disk by the magnetic field applied by a transducer embedded in the trailing edge of the flying magnetic head. Both the disk and the head are coated with an ultrathin *a*-C film for protection against impact, wear, and corrosion, which is critical to the longevity of HDDs [4–5]. The structure of *a*-C films is characterized by two main types of atomic carbon bonding – graphite-like and diamond-like (DLC), often referred to as sp^2 and sp^3 hybridizations, respectively. The σ-bond exists only in sp^3 hybridizations and is stronger than the π-bond. It is recognized that sp^3 hybridization controls the mechanical properties, while sp^2 hybridization is mainly responsible for the electrical and optical properties [1], [6]. The high hardness of *a*-C films is closely related to the sp^3 content, with higher sp^3 content usually correlating with better film protection [7], [8].

The most common methods for synthesizing ultrathin *a*-C films are filtered cathodic vacuum arc (FCVA) [8], [9], pulsed laser deposition [8], [10], chemical vapor deposition [8], [11], [12], and sputtering [13]. Depending on the deposition process and the range of controlling process parameters (e.g., plasma power, substrate bias voltage, and ion fluence), *a*-C films possessing different microstructures and mechanical properties can be deposited on various substrates [1–3], [9]. Among the previous methods, FCVA is more advantageous because it is a cost-effective technique for depositing ultrathin, hydrogen-free *a*-C films with high sp^3 contents, also known as tetrahedral *a*-C films [1]. Because *a*-C films demonstrate a hardness of ~80 GPa and an elastic modulus in the range of 710–805 GPa, they are ideal protective overcoats for mechanical wear [14], [15]. Even in high-temperature environments, tetrahedral *a*-C films perform better than carbon films with lower sp^3 contents [16]. In fact, *a*-C films synthesized by FVCA demonstrate thermal stability even under the intense localized heating

induced by a pulsed laser and, therefore, are suitable overcoats for emerging new technologies of information storage, such as energy-assisted magnetic recording [17].

To achieve magnetic storage levels of 10 Tb/in^2 and beyond in next-generation HDDs, the physical gap between the magnetic head and the hard disk must be reduced to less than 2-4 nm, implying an overcoat thickness of less than ~2 nm. It is critical that this significant decrease in overcoat thickness does not lead to the loss of important film properties, such as high sp^3 content, low surface roughness (≤0.2 nm), and high hardness (>40 GPa). However, traditional deposition methods, such as sputtering, cannot produce continuous ultrathin *a*-C films of such high quality. FCVA is a promising alternative method that allows for the deposition of continuous *a*-C films less than 2 nm in thickness. In FCVA, the film precursors are energetic ions which impinge onto the substrate surface resulting in implantation, recoil implantation, and deposition, depending on the process conditions (e.g., substrate pulsed bias voltage). A common approach for depositing ultrathin films is to decrease the ion energy and/or the deposition time, which is equivalent to decreasing the total number of ions arriving at the surface of the growing film. However, because the film quality depends strongly on the ion energy, decreasing the ion energy may be detrimental to the film properties [1], [9]. Varying the incident angle of bombarding ions is more advantageous because the effect on the film microstructure and properties is secondary compared to that due to changes in the ion energy or ion fluence [18]. Consequently, an alternative approach for ultrathin *a*-C film deposition by the FCVA method might be to vary the incident angle of the impinging ions θ (defined as the angle between the trajectory of the C^+ ions and the substrate normal) while maintaining the desired C^+ ion energy. This method is referred to as oblique deposition and is depicted schematically in Fig. 1.

Oblique deposition has been used to synthesize films of specific surface structure or orientation on patterned substrates, such as nanoimprinted solar cells [19] and fibers [20], [21]. However, fundamental studies of the effect of oblique deposition on smooth substrates are sparse. In particular, knowledge of the incident angle effect on the quality and thickness of ultrathin *a*-C films is limited. Cuome *et al*. [18] studied the effect of incident angle on the quality of DLC films deposited by various methods and

observed a sharp decrease in the sp^3 content of DLC films deposited by pulsed laser vaporization for incident angles larger than 45°; however, an incident angle effect on the sp^3 content of DLC films deposited by FCVA was not reported. Liu *et al.* [22] used pulsed cathodic arc to deposit DLC films of thickness in the range of 60–120 nm and discovered that ~100-nm-thick DLC films possessed lower sp^3 contents and higher roughness for incident angles above 80° and below 50°, respectively. Raman spectroscopy studies of Liu *et al.* [23] have shown significantly lower internal stresses in DLC films deposited at large incident angles; however, the effect on the hardness was less significant, while the film structure was not examined in the light of direct microanalysis results [24].

The objective of the present study was to examine the effect of the incident angle of energetic carbon ions on the thickness, morphology (roughness), and structure of ultrathin *a*-C films deposited by the FCVA method. Film depth profiles were determined from Monte Carlo simulations and cross-section transmission electron microscopy (TEM), while the topography (roughness) and structure of the films were examined by atomic force microscopy (AFM) and X-ray photoelectron spectroscopy (XPS), respectively.

II. EXPERIMENTAL AND SIMULATION PROCEDURES

A. Film Deposition System

Fig. 1 shows a schematic of the FCVA system used in this study. Arcing generated by a mechanical trigger between the cathode (99.99% pure graphite)) and the anode resulted in the carbon expulsion from the cathode in the plasma state. The carbon plasma was stabilized by a cusp-configuration magnetic field applied to the cathode [25]. An S-shaped duct configuration with electromagnetic coils was used to filter the plasma from macroparticles and/or droplets that could be expelled from the cathode during arcing. Under the current plasma conditions, the produced film precursors comprised only high-purity (~99.99%) C^+ ions. To vary the ion incident angle and to enhance the film uniformity in the radial direction, the substrate was tilted and rotated at 60 rpm.

During FCVA deposition, collision cascades between C^+ ions and substrate atoms lead to sp^3 hybridization, whereas thermal relaxation promotes $sp^3 \rightarrow sp^2$ rehybridization. Although the sp^3 fraction increases with the C^+ ion energy, thermal relaxation becomes an important factor at high ion energy levels. Therefore, there is an optimum ion energy (typically equal to ~120 eV [1]) for producing carbon films of highest sp^3 content. Because the energy of the C^+ ions generated by arcing is ~20 eV, a bias voltage of –100 V was applied to the substrate during FCVA deposition (Fig. 1) to increase the energy of impinging C^+ ions. Substrates (10 × 10 mm^2) cut from a p-type Si(100) wafer were first cleaned with acetone and then by Ar^+ ion sputter etching of 500 eV power and 60° incident angle for 2 min to remove the native oxide film. In all depositions, the base and working pressures were less than 8×10^{-7} and 1×10^{-4} Torr, respectively, while the deposition time was fixed at 30 s.

Cross-sections of films deposited at incident angles in the range of 0–70° were examined with the TEM (Philips CM200/FEG). Cross-section TEM samples were prepared by mechanical grinding and dimpling. Film samples were cleaved into two halves and glued face-to-face using M-bond 610 epoxy. After curing at 160 ^{o}C for 1 h, Si(100) was glued to both sides of the sandwiched film samples to increase the sample thickness to >3 mm. These samples were then sectioned in 500-μm-thick slices with a diamond blade and saw-cut to disks of 3 mm in diameter. Finally, the disks were ground down to a thickness of 5–8 μm at the center by double-side dimpling and ion milled from the top and the bottom with Ar^+ guns operated at 5 kV and 5 mA (Fischione Instruments, Export, PA) to produce a through-thickness hole across the interface. High-resolution TEM images were obtained at 200 keV with a spatial resolution of 1 nm.

Depth profiles of the deposited films were simulated with the TRIM-DYNAMIC (T-DYN) code (version 4.0) [26], [27], a Monte Carlo simulator based on the classical trajectory method that accounts for binary collision during deposition. Simulations were performed for ion energy equal to 120 eV, similar to that used for film deposition. The binding energy and surface binding energy of Si were set equal to 2.32 and 4.7 eV and those of carbon to 2.27 and 7.41 eV, respectively [28], [29]. The ion incident

angle was varied between 0° and 85° at 5° increments. The accuracy of the simulated depth profiles was confirmed by comparing with TEM results.

The sp^3 content of the films was determined from XPS measurements obtained with a PHI 5400 system (Physical Electronics, Chanhassen, MN), using non-monochromatic Al-Kα radiation of 1486.6 eV energy and work function of 5.7 eV, under a vacuum pressure of less than 2×10^{-8} Torr. The system has a spatial resolution of 0.5 mm and energy resolution of 0.7 eV. Sample cleaning before the XPS analysis was not performed to preserve the surface elemental and chemical state of the sample surfaces. Multiplex narrow-scan spectra of the C1s peak were acquired with pass energy of 37.75 eV, using a channel width of 0.1 eV/step and acquisition time fixed at 50 ms/step. Spectra were collected after 50 sweeps in the binding energy range of 280–292 eV.

The film topography was examined in light of 1×1 μm^2 surface area images obtained with an AFM (Dimension 3100, Digital Instrument) operated in the tapping mode at a drive frequency of 278.244 Hz. AFM imaging was performed with Si tips of nominal radius less than 10 nm at a scanning speed of ~3.9 μm/s. All AFM samples were cleaned with acetone before scanning. For statistical analysis, three different surface locations of two *a*-C films deposited under identical FCVA conditions were imaged with the AFM, and the obtained roughness data were assumed to follow a normal distribution.

III. Results and Discussion

Fig. 2 shows cross-section TEM images of *a*-C films deposited at different incident angles. The periodic array of the substrate is illustrative of the single-crystal structure of Si(100). Fast Fourier transform analysis showed that, in all images, the zone axis is in the [110] direction of the silicon lattice due to sample titling. The TEM images shown in Figs. 2(a)–2(c) reveal a three-layer structure consisting of a crystalline Si(100) substrate, an intermixing layer, and a carbon film. The structure regularity decreases near the interface of the substrate with the intermixing layer and disappears in the film, indicative of the amorphous structure of the carbon film. The contrast between the intermixing layer and the bulk of the *a*-C film indicates that the intermixing layer is at a different stress state and possesses a

different chemical composition than the *a*-C film. From the contrast difference, the thickness of the intermixing layer is estimated to be equal to ~3.5 nm, which is in good agreement with previous studies [30]. A comparison of the TEM images shows a significantly smaller *a*-C film thickness for a relatively large incident angle (i.e., θ = 60° and 70°). For the largest incident angle of 70°, in particular, it is difficult to distinguish the three-layer structure observed with smaller incident angles. The TEM image shown in Fig. 2(d) suggests the formation of an ultrathin *a*-C film at very large incident angles (i.e., $\theta \geq$ 70°), apparently due to excessive sputtering.

Fig. 3 shows carbon depth profiles simulated with the T-DYN code for incident angle between 0° and 75° and C^+ ion fluence equal to 0.9×10^{16}, 4.5×10^{16}, and 9.0×10^{16} ions/cm^2, corresponding to 0.1, 0.5, and 1 min deposition time. Short deposition time (low ion fluence) mainly leads to carbon ion implantation into the silicon substrate, resulting in the formation of a Si–C intermixing layer (Fig. 3(a)). However, increasing the deposition time produces a three-layer structure consisting of a carbon film, an intermixing layer, and a silicon substrate (Fig. 3(b)). Further increasing the deposition time increases the thickness of the carbon film without affecting the thickness of the intermixing layer (Fig. 3(c)). The decrease of the carbon film thickness with the ion fluence is due to the availability of less C^+ ions. For all deposition times (or ion fluence) and ion kinetic energy fixed at 120 eV, the depth of the carbon profile decreased with the increase of the incident angle, evidently due to the decrease of the C^+ ion velocity normal to the substrate surface, which, in turn, decreased the depth travelled by recoil carbon atoms.

Fig. 4 shows T-DYN simulation results of the total carbon thickness (0–100 at% C) and the intermixing layer thickness (0–90 at% C) as functions of incident angle and ion fluence. The region of 90–100 at% C is presumed to represent the carbon film. For small incident angle (i.e., $\theta < 30°$), ion-surface interaction was localized (i.e., limited surface diffusion of carbon) due to the low in-plane velocity of the impinging C^+ ions. However, the significant increase of the in-plane ion velocity for $\theta > 30°$ promoted C–Si and C–C collisions. This non-local effect led to the decrease of the total carbon thickness (Fig. 4(a)) and, in particular, the thickness of the intermixing layer (Fig. 4(b)) with the increase of the

incident angle above 30°. In addition to the incident angle, the C^+ ion fluence (deposition time) also affected the thickness of total carbon and intermixing layer, although the latter effect diminished at ion fluences above 4.5×10^{16} ions/cm^2 (deposition times >0.5 min).

Fig. 5(a) shows simulation results of the deposition yield Y (i.e., fraction of C^+ ions deposited and/or implanted into the Si substrate) for different incident angles. The relative deposition yield for a given incident angle θ and C^+ ion energy E is defined as the ratio $Y(E, \theta)/Y(E, \theta = 0)$. The minimum deposition yield occurs at $\theta_{min} = 72.8°$, and the effect of the C^+ ion fluence is shown to be secondary. Similar to ion sputtering [31], [32], the deposition yield is mainly controlled by two factors – the ion fluence I and the ion penetration depth. Thus, Y decreases continuously with the increase of θ because $I = I_0 \cos\theta$, where I_0 is the total C^+ ion fluence; however, above a critical θ value (~75°–80°), the increased in-plane velocity of the impinging C^+ ions intensified the C–Si atomic collisions, resulting in the entrapment of carbon and, hence, the increase of Y (Fig. 5(a)). According to sputtering theory [32],

$$\frac{1-Y(E,\theta)}{1-Y(E,\theta=0)} = \exp\left(\frac{\sin^2\theta}{2\cos^2\theta_{min}}\right)\cos\theta \qquad (1)$$

where θ_{min} is the incident angle corresponding to the minimum deposition yield. The good agreement between simulation results and Eq. (1) confirms the weak C^+ ion fluence effect on deposition yield. Fig. 5(b) shows a comparison between deposition yield results obtained from T-DYN simulations and TEM measurements. The film thickness for $\theta = 0°$ was used as a reference. Fitting the deposition yield data determined from the TEM measurements and using $\theta_{min} = 72.8°$, the normal incidence yield rate $Y(E, \theta = 0)$ in Eq. (1) was found equal to 0.9835, which is slightly lower than the 0.9904 value obtained from the T-DYN analysis. Fig. 5(b) shows a good agreement between TEM and simulation results, except for large θ values. This discrepancy may be attributed to the true dose of C^+ ions arriving at the sample surface at large incident angles ($\theta > 80°$).

Further insight into the effect of the incident angle on the film quality can be obtained from the XPS and AFM results presented next. Fig. 6 shows typical XPS C1s core level peaks of *a*-C films deposited at

an incident angle of 60° (Fig. 6(a)) and 0° (Fig. 6(b)) for a deposition time of 0.5 min, i.e., 4.5×10^{16} ions/cm^2 ion fluence. After performing a Shirley inelastic background subtraction, each C1s peak was fitted with five Gaussian distributions, namely C1s-1, C1s-2, and C1s-3 corresponding to sp^1, sp^2, and sp^3 carbon-carbon hybridization, respectively, and C1s-4 and C1s-5 representing high-order C–O and C=O bonds, respectively. The binding energy of each carbon chemical state was assigned the peak energy of the corresponding Gaussian distribution. The sp^2 and sp^3 fractions are defined as the area of the C1s-2 and the C1s-3 distributions, respectively, divided by the sum of the areas of the C1s-2 and C1s-3 distributions.

Fig. 7(a) shows XPS measurements of the binding energy of sp^3 and sp^2 carbon atom hybridizations in terms of the incident angle. A shift in the binding energy is normally associated with the presence of an internal (intrinsic) stress, with a compressive (tensile) stress resulting in the decrease (increase) of the binding energy [33]. For $\theta < 45°$, the binding energies of both sp^2 and sp^3 hybridizations are close to those for $\theta = 0°$. However, the binding energy of sp^3 hybridization for $\theta = 60°$ is larger than that for $\theta = 0°$, indicating a lower compressive stress in the film. Experiments and Monte Carlo simulations have shown that sp^3 and sp^2 carbon bonds are usually under compression and tension, respectively [1], [34]. Therefore, the lower compressive stress in the *a*-C film deposited at $\theta = 60°$ may be correlated to a lower sp^3 fraction. This is confirmed by the significant decrease in sp^3 fraction shown in Fig. 7(b). Because of strong dependence of the hardness on sp^3 carbon atom hybridization and the small variation of sp^3 content in the range $0° \leq \theta \leq 45°$, it may be inferred that the *a*-C films deposited at these incident angles should exhibit similar hardness and wear resistance.

In addition to the mechanical properties of the *a*-C films, the surface roughness is also of high importance because it controls the probability of asperity-asperity interaction at low flying heights. Higher friction and faster wear are normally encountered with increasing surfaces roughness. For a two-dimensional surface profile $y(x)$, the root-mean-square roughness R_q is defined as

$$R_q = \left[\frac{1}{n}\sum_{i=1}^{n} y_i^2\right]^{\frac{1}{2}} \tag{2}$$

where y_i represents the height of the ith point of the surface profile from the mean plane (y = 0), and n is the number of height measurements. Fig. 8 shows the *a*-C film roughness as a function of incident angle. As a reference, the R_q roughness of the Si(100) after Ar^+ sputter cleaning was equal to ~0.143 nm. For small incident angle ($\theta < 30°$), the roughness increased with the incident angle due to the dominance of ion sputter etching induced by the increase of the in-plane velocity of impinging C^+ ions. Increasing the incident angle above 30° led to the decrease in film roughness to a minimum value (~0.15 nm) at $\theta = 45°$, attributed to a balance between deposition and sputtering processes. For $\theta > 45°$, R_q increased with θ due to the dominance of sputtering. Despite the prevalence of different mechanisms in the three ranges of incident angle show in Fig. 8, the film roughness was not affected significantly by the variation of the incident angle.

The R_q roughness represents a statistical measurement of the average deviation of the surface heights from the mean plane. Further insight into the film surface topography can be obtained by considering the higher moments of the surface height profile, such as skewness S and kurtosis K, defined as

$$S = \frac{1}{nR_q^3}\sum_{i=1}^{n} y_i^3 \qquad (3)$$

$$K = \frac{1}{nR_q^4}\sum_{i=1}^{n} y_i^4 \qquad (4)$$

Skewness is a measure of the lack of symmetry of the probability distribution of surface heights. A positive skewness implies a small fraction of asperities with heights above the mean height, whereas a negative skewness implies that a surface topography dominated by valleys than asperities. Considering that the probability of asperity interaction is lower for $S > 0$ than for $S < 0$, significantly different tribological behaviors may be encountered with surfaces possessing similar R_q but different S values. Obviously, $S > 0$ is preferred in ultralow-flying height HDDs. The Kurtosis is a measure of variance, i.e., it indicates how tightly the peaks (asperities) and valleys of the surface profile are relative to the mean height value. For normal distribution, $S = 0$ and $K = 3$. Fig. 9 shows that, with the exception of $\theta = 15°$, the incident angle did not affect the variance of the surface height distribution of the *a*-C films. However,

the skewness results indicate that the most desirable surface topographies were obtained for $\theta = 0°$ and 45°. Thus, when Figs. 8 and 9 are considered together, it may be inferred that, from a surface topography perspective, the optimum incident angle is 45°.

IV. Conclusion

Ultrathin *a*-C films were deposited by the FCVA method at different incident angles of energetic C^+ ions. Numerical results confirmed by TEM measurements showed that the *a*-C film thickness decreases with the incident angle, while the deposition yield (rate) is independent of the ion fluence and obeys a relationship derived from sputtering theory. XPS and AFM results demonstrated that the sp^3 fractions and topographies of *a*-C films deposited at incident angles less than 45° were similar to those of films deposited at 0° incident angle. Considering the effects of the incident angle on the thickness, structure, and topography of the deposited *a*-C films, the optimum incident angle for FCVA deposition is 45°. The results of this study indicate that, depending on the C^+ ion fluence, *a*-C films of thickness only a few nanometers can be obtained by oblique (45° incident angle) FCVA deposition.

Acknowledgment

This research was funded by the Computer Mechanics Laboratory (CML) and the UCB-KAUST Academic Excellence Alliance (AEA) Program. TEM and XPS studies were performed at the National Center for Electron Microscopy and Molecular Foundry, respectively, Lawrence Berkeley National Laboratory, supported by the Director, Office of Science, Office of Basic Energy Sciences of the U.S. Department of Energy under Contract No. DE-AC02-05CH11231.

References

[1] J. Robertson, “Diamond-like amorphous carbon,” *Mater. Sci. Eng. R*, vol. 37, pp. 129–281, 2002.

[2] A. Grill, “Diamond-like carbon: state of the art,” *Diam. Relat. Mater.*, vol. 8, pp. 428–434, 1999.

[3] R. Hauert, “An overview on the tribological behavior of diamond-like carbon in technical and medical applications,” *Tribol. Int.*, vol. 37, pp. 991–1003, 2004.

[4] M. H. Kryder, E. C. Gage, T. W. McDaniel, W. A. Challener, R. E. Rottmayer, G. Ju, Y.-T. Hsia, and M. F. Erden, "Heat assisted magnetic recording," *Proc. IEEE*, vol. 96, pp. 1810–1835, 2008.

[5] N. Yasui, H. Inaba, K. Furusawa, M. Saito, and N. Ohtake, "Characterization of head overcoat for 1 Tb/in^2 magnetic recording," *IEEE Trans. Magn.,* vol. 45, pp. 805–809, 2009.

[6] J. Diaz, G. Paolicelli, S. Ferrer, and F. Comin, "Separation of the sp^3 and sp^2 components in the C1s photoemission spectra of amorphous carbon films," *Phys. Rev. B*, vol. 54, pp. 8064–8069, 1996.

[7] D. R. McKenzie, "Tetrahedral bonding in amorphous carbon," *Rep. Prog. Phys.*, vol. 59, pp. 1611–1664, 1996.

[8] O. R. Monteiro, "Thin film synthesis by energetic condensation," *Annu. Rev. Mater. Res.,* vol. 31, pp. 111–137, 2001.

[9] I. G. Brown, "Cathodic arc deposition of film," *Annu. Rev. Mater. Sci.,* vol. 28, pp. 243–269, 1998.

[10] A. A. Voevodin and M. S. Donley, "Preparation of amorphous diamond-like carbon by pulsed laser deposition: a critical review," *Surf. Coat. Technol.,* vol. 82, pp. 199–213, 1996.

[11] M. K. Fung, K . H. Lai, C. Y. Chan, I. Bello, C. S. Lee, S. T. Lee, D. S. Mao, and X. Wang, "Mechanical properties and corrosion studies of amorphous carbon on magnetic disks prepared by ECR plasma technique," *Thin Solid Films,* vol. 368, pp. 198–202, 2000.

[12] Q. W. Leng, H. Han, M. Mao, C. Hiner, and F. Ryan, "Magnetic dead layer in NiHe/Ta and NiFe/Si/diamond-like carbon films," *J. Appl. Phys.,* vol. 87, pp. 6621–6623, 2000.

[13] D. Wan and K. Komvopoulos, "Probabilistic analysis of tertrahedral carbon hybridization in amorphous carbon films," *Appl. Phys. Lett.,* vol. 88, pp. 221908(1-3), 2006.

[14] H. D. Espinosa, B. Peng, N. Moldovan, T. A. Friedmann, X. Xiao, D. C. Mancini, O. Auciello, J. Carlisle, C. A. Zorman, and M. Merhegany, "Elasticity, strength and toughness of single crystal silicon carbide, ultrananocrystalline diamond, and hydrogen-free tetrahedral amorphous carbon," *Appl. Phys. Lett.,* vol. 89, pp. 073111(1-3), 2006.

[15] D. S. Grierson, A. V. Sumant, A. R. Konicek, T. A. Friedmann, J. P. Sullivan, and R. W. Carpick, "Thermal stability and rehybridization of carbon bonding in tetrahedral amorphous carbon," *J. Appl. Phys.,* vol. 107, pp.033523(1-5), 2010.

[16] S. Anders, J. Diaz, J. W. Agger III, R. Y. Lo, and D. B. Bogy, "Thermal stability of amorphous hard carbon films produced by cathodic arc deposition," *Appl. Phys. Lett.*, vol. 71, pp. 3367–3369, 1997.

[17] N. Wang and K. Komvopoulos, "Thermal stability of ultrathin amorphous carbon films for energy-assisted magnetic recording," *IEEE Trans. Magn.*, vol. 47, pp. 2277–2282, 2011.

[18] J. J. Cuomo, D. L. Pappas, R. Lossy, J. P. Doyle, J. Bruley, G. W. Di Bello, and W. Krakow, "Energetic carbon deposition at oblique angles," *J. Vac. Sci. Technol. A*, vol. 10, pp. 3414–3418, 1992.

[19] Y. Yang, M. Aryal, K. Mielczarek, W. Hu, and A. Zakhidov, "Nanoimprinted P3HT/C_{60} solar cells optimized by oblique deposition of C_{60}," *J. Vac. Sci. Techol. B*, vol. 28, pp. 1071–1023, 2010.

[20] M. Yusop, K. Yamaguchi, T. Suzuki, and P. Ghosh, "Morphology and size of ion induced carbon nanofibers: effect of ion incidence angle, sputtering rate and temperature," *Jap. J. Appl. Phys.,* vol. 50, pp.01AF10–6, 2011.

[21] S. Jayawardhanna, G. Kostovski, A. Mazzolini, and P. Stoddart, "Optical fiber sensor based on oblique angle deposition," *Appl. Optics*, vol. 50, pp. 155–162, 2011.

[22] D. Liu, G. Benstetter, E. Lodermeier, and J. Vancea, "Influence of the incident angle of energetic carbon ions on the properties of tetrahedral amorphous carbon (ta-C) films," *J. Vac. Sci. Tech. A*, vol. 21, pp. 1665–1670, 2003.

[23] F. X. Liu, K. L. Yao, and Z. L. Liu, "Substrate tilting effect on structure of tetrahedral amorphous carbon films by Raman spectroscopy," *Surf. Coat. Technol.,* vol. 201, pp. 7235–7240, 2007.

[24] F. X. Liu and Z. L.Wang, "Thickness dependence of the structure of diamond-like carbon films by Raman spectroscopy," *Surf. Coat. Technol.,* vol. 203, pp. 1829–1832, 2009.

[25] H. S. Zhang and K. Komvopoulos, "Direct-current cathodic vacuum arc system with magnetic field mechanism for plasma stabilization," *Rev. Sci. Instrum.*, vol. 79, pp. 073905(1-7), 2008.

[26] J. Biersack, S. Berg, and C. Nender, "T-DYN Monte Carlo simulations applied to ion assisted thin film processes," *Nucl. Instrum. Meth. Phys. Res. B*, vol. 59/60, pp. 21–27, 1991.

[27] J. Biersack, "TRIM-DYNAMIC applied to marker broadening and SIMS depth profiling," *Nucl. Instrum. Methods Phys. Res. B*, vol. 153, pp. 398–409, 1999.

[28] H. S. Zhang and K. Komvopoulos, "Synthesis of ultrathin carbon films by direct current filtered cathodic vacuum arc," *J. Appl. Phys.,* vol. 105, pp. 083305-1–083305-7, 2009.

[29] W. M. Haynes, *CRC Handbook of Chemistry and Physics*, 92nd ed., CRC Press, New York, 2011.

[30] M. P. Siegal, P. N. Provencio, D. R. Tallant, and R. L. Simpson, "Bonding topologies in diamondlike amorphous-carbon films," *Appl. Phys. Lett.*, vol. 76, pp. 2047–2049, 2000.

[31] P. Sigmund, "Theory of sputtering. I. Sputtering yield of amorphous and polycrystalline targets," *Phys. Rev.*, vol. 184, pp. 383–416, 1969.

[32] Q. Wei, K.-D. Li, J. Lian, and L. Wang, "Angular dependence of sputtering yield of amorphous and polycrystalline materials," *J. Phys. D: Appl. Phys.*, vol. 41, pp. 17002(1-4), 2008.

[33] D. Wan and K. Komvopoulos, "Tetrahedral and trigonal atom hybridization in thin amorphous carbon films synthesized by radio-frequency sputtering," *J. Phys. Chem. C*, vol. 111, pp. 9891–9896, 2007.

[34] P. C. Kelires, "Intrinsic stress and stiffness variations in amorphous carbon," *Diam. Relat. Mater.*, vol. 10, pp. 139–144, 2001.

List of Figures

Fig. 1 Schematic of filtered cathodic vacuum arc (FCVA) system. The incident angle θ of C^+ ions impinging onto the substrate is the angle between the ion trajectory and the substrate normal.

Fig. 2 Cross-section TEM images of carbon films deposited at an incident angle equal to (a) 0°, (b) 45°, (c) 60°, and (d) 70°. (White lines demarcate the interfaces between Si(100) substrate, intermixing layer, *a*-C film, and epoxy mounting material.)

Fig. 3 Depth profiles of carbon films simulated with the T-DYN code for different incident angles and C^+ ion dose equal to (a) 0.9×10^{16}, (b) 4.5×10^{16}, and (c) 9.0×10^{16} ions/cm^2 and corresponding deposition time of 0.1, 0.5, and 1 min.

Fig. 4 (a) Total thicknesses of carbon and (b) thickness of intermixing layer of carbon film deposition simulated with the T-DYN code for different incident angles and C^+ ion fluence in the range of $(0.9–9.0)\times10^{16}$ ions/cm^2.

Fig. 5 Deposition yield versus incident angle and ion dose obtained from (a) T-DYN simulations and (b) TEM thickness measurements. Both simulation and experimental results are in good agreement with sputtering theory (Eq. (1)).

Fig. 6 XPS spectra of the C1s core level peak of *a*-C films for an incident angle of (a) 60° and (b) 0°, ion kinetic energy fixed at 120 eV (–100 V substrate bias), and deposition time equal to 0.5 min (4.5×10^{16} ions/cm^2 ion fluence). The spectra were fitted with five Gaussian distributions after Shirley background subtraction.

Fig. 7 Variation of (a) binding energy of sp^2 and sp^3 carbon atom hybridizations and (b) sp^3 fraction of *a*-C films with incident angle. (The experimental conditions are the same as those in Fig. 6. Error bars indicate one standard deviation above and below the corresponding mean value.)

Fig. 8 Root-mean-square roughness versus incident angle. (Error bars indicate one standard deviation above and below the corresponding mean value.)

Fig. 9 Skewness and kurtosis versus incident angle. (Error bars indicate one standard deviation above and below the corresponding mean value.)

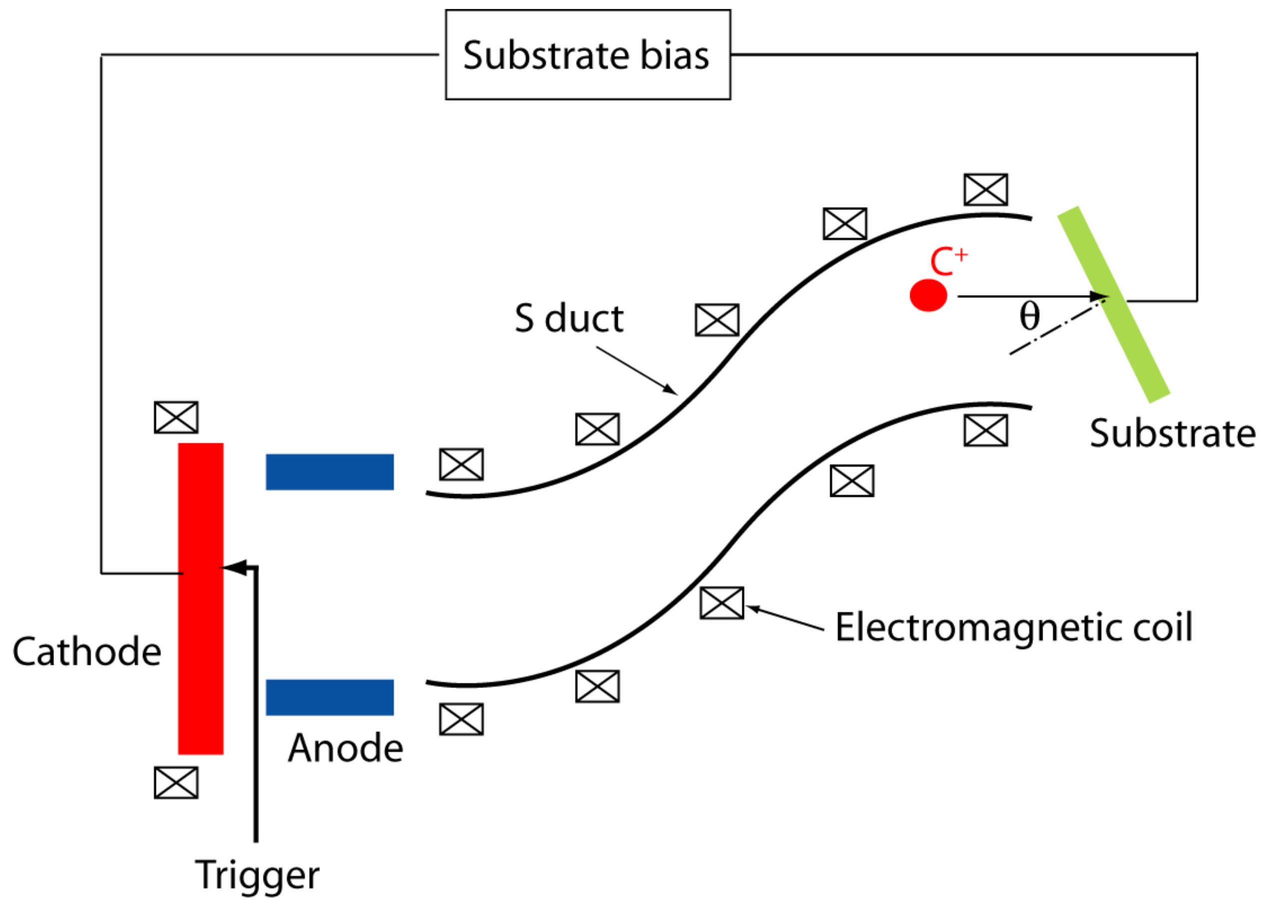

Figure 1

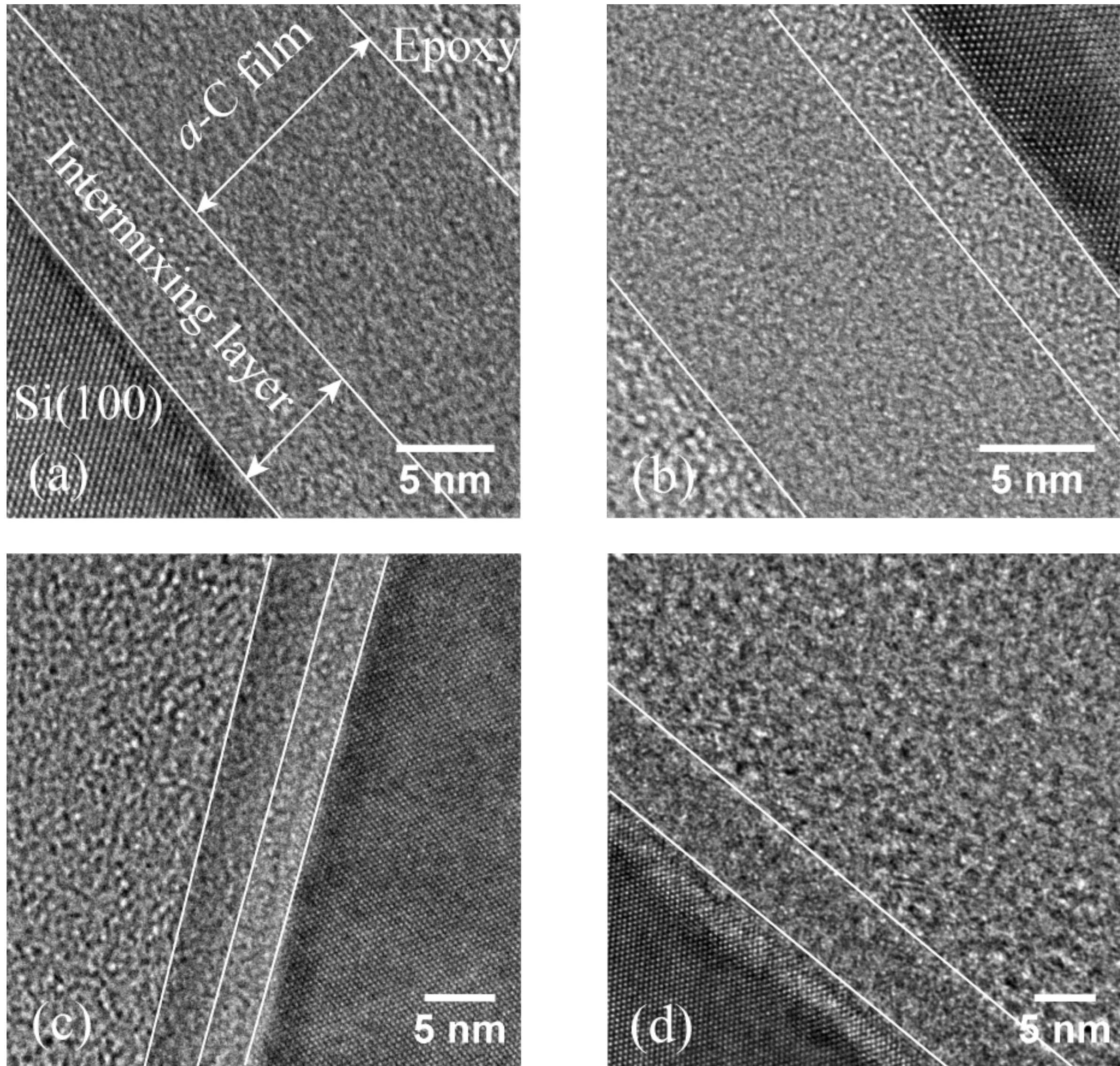

Figure 2

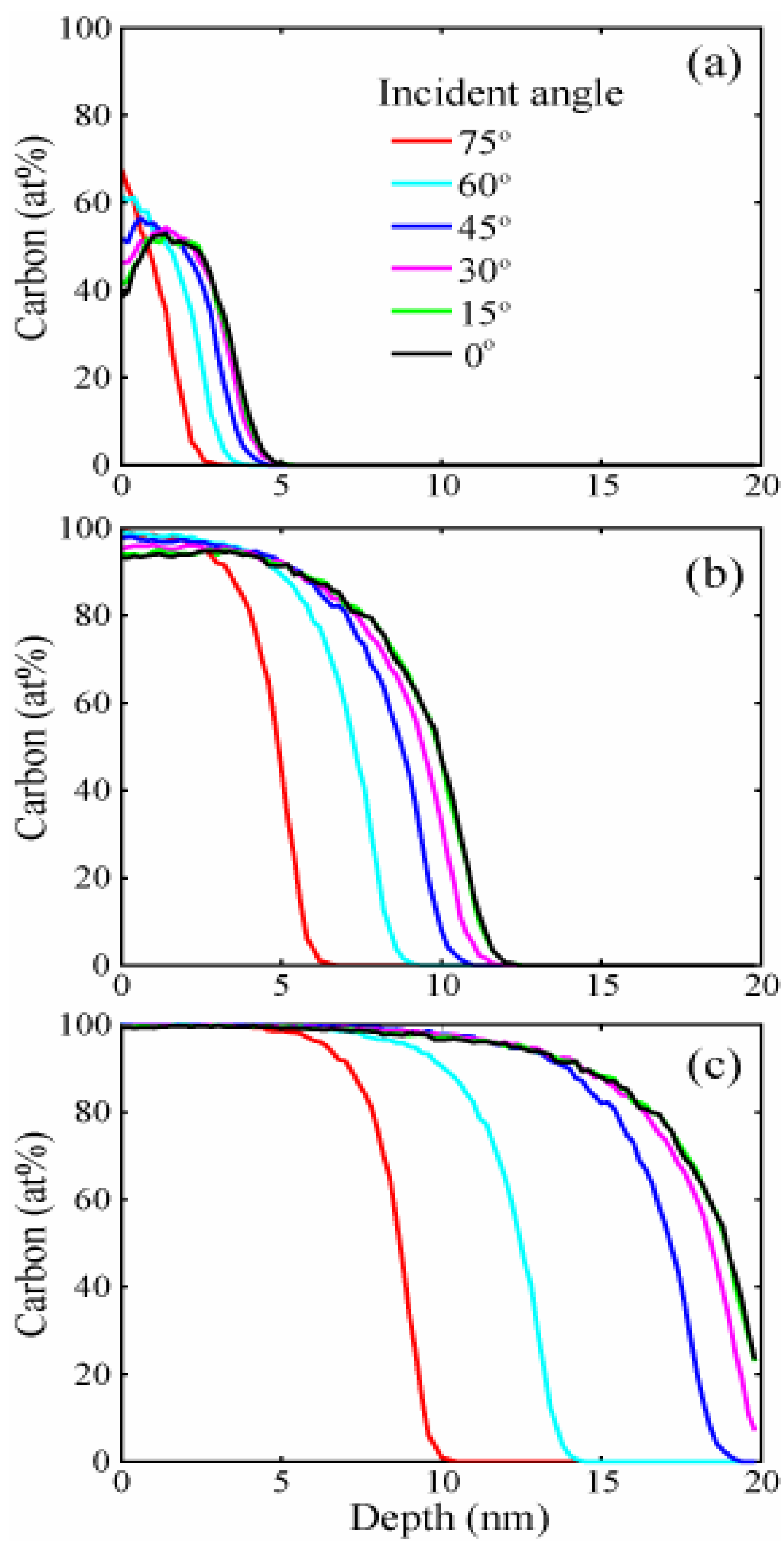
(a)
Incident angle
75°
60°
45°
30°
15°
0°
Carbon (at%)
(b)
(c)
Depth (nm)

Figure 3

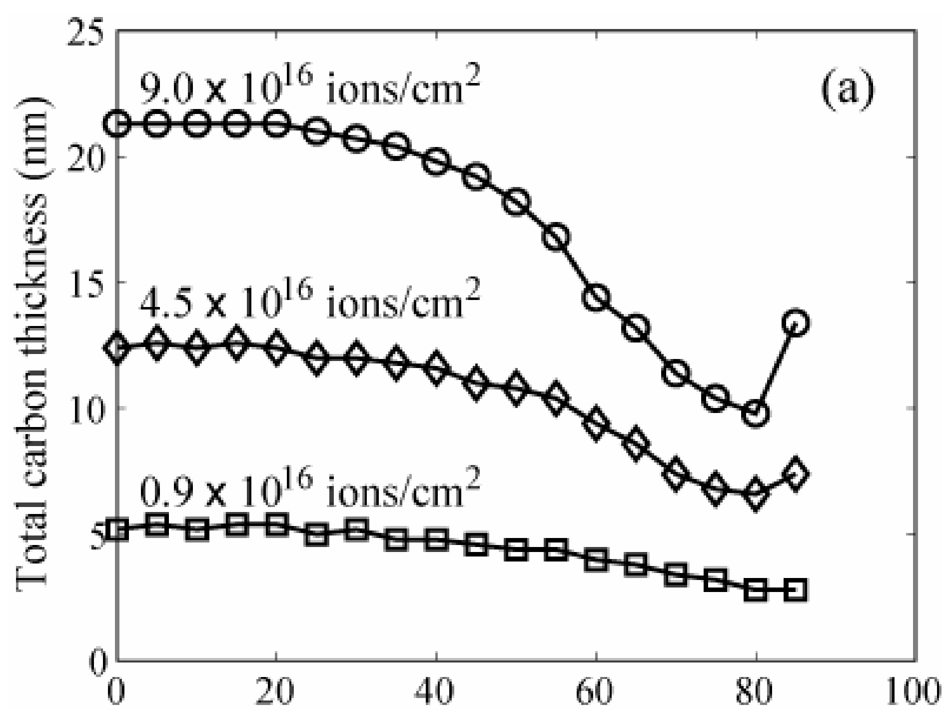

25
20
15
10
5
0
Total carbon thickness (nm)
9.0 x 10^16 ions/cm^2
4.5 x 10^16 ions/cm^2
0.9 x 10^16 ions/cm^2
(a)
0
20
40
60
80
100

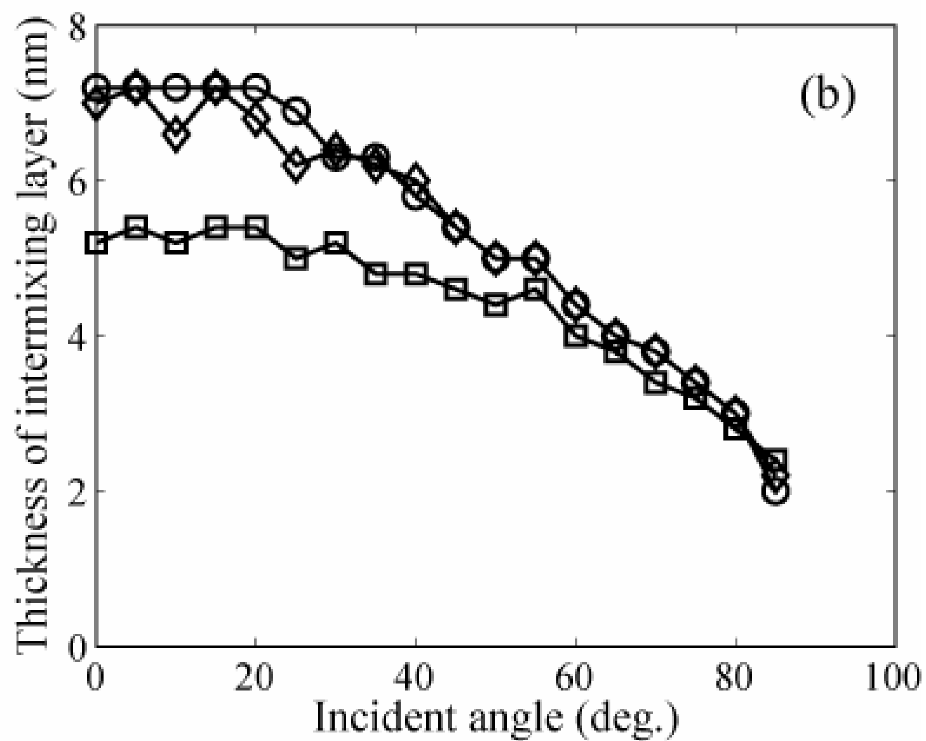

8
6
4
2
0
Thickness of intermixing layer (nm)
(b)
0
20
40
60
80
100
Incident angle (deg.)

Figure 4

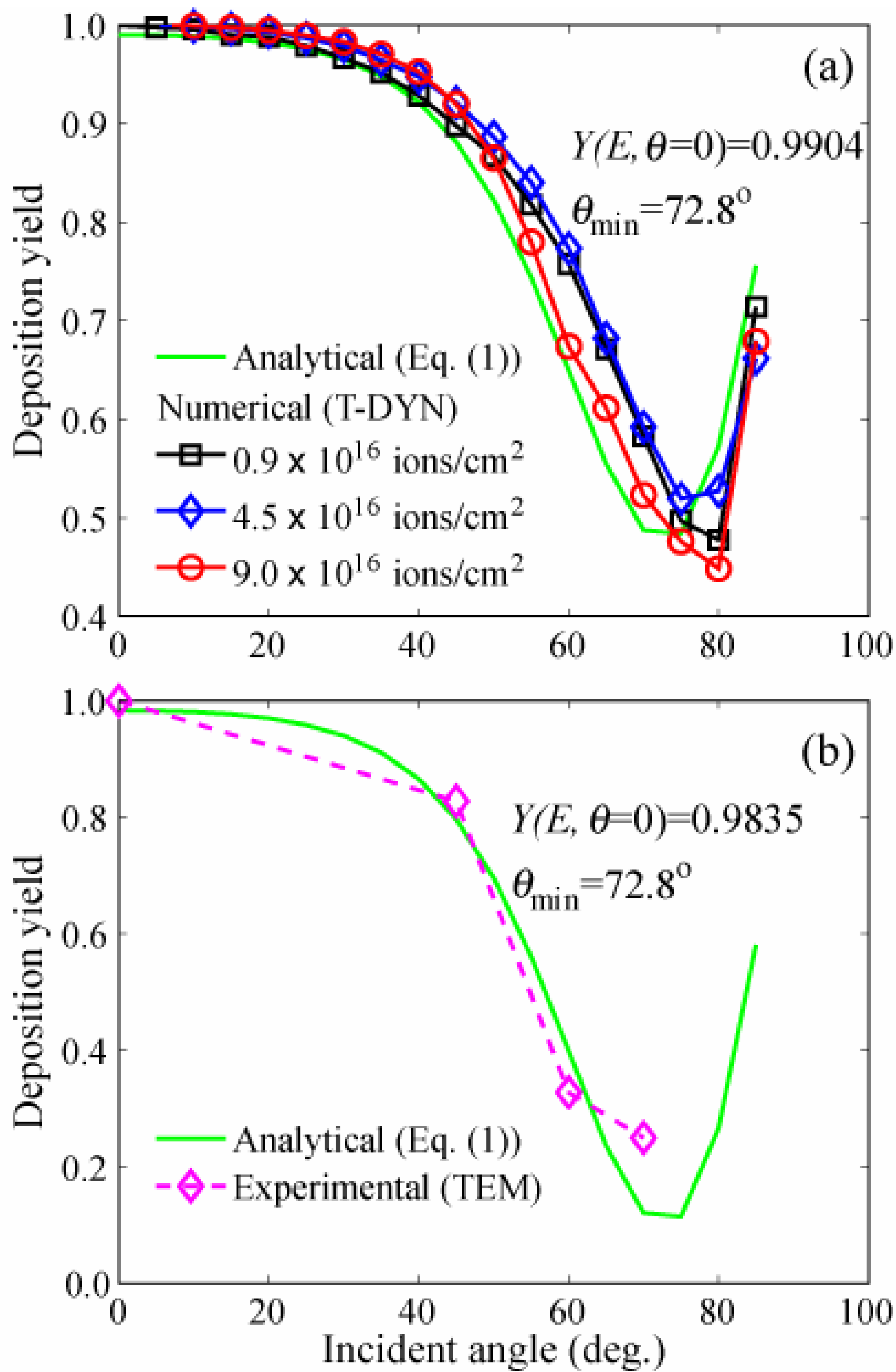

(a)
Y(E, θ=0)=0.9904
θmin=72.8°
Deposition yield
Analytical (Eq. (1))
Numerical (T-DYN)
0.9 x 10^16 ions/cm^2
4.5 x 10^16 ions/cm^2
9.0 x 10^16 ions/cm^2
(b)
Y(E, θ=0)=0.9835
θmin=72.8°
Deposition yield
Analytical (Eq. (1))
Experimental (TEM)
Incident angle (deg.)

Figure 5

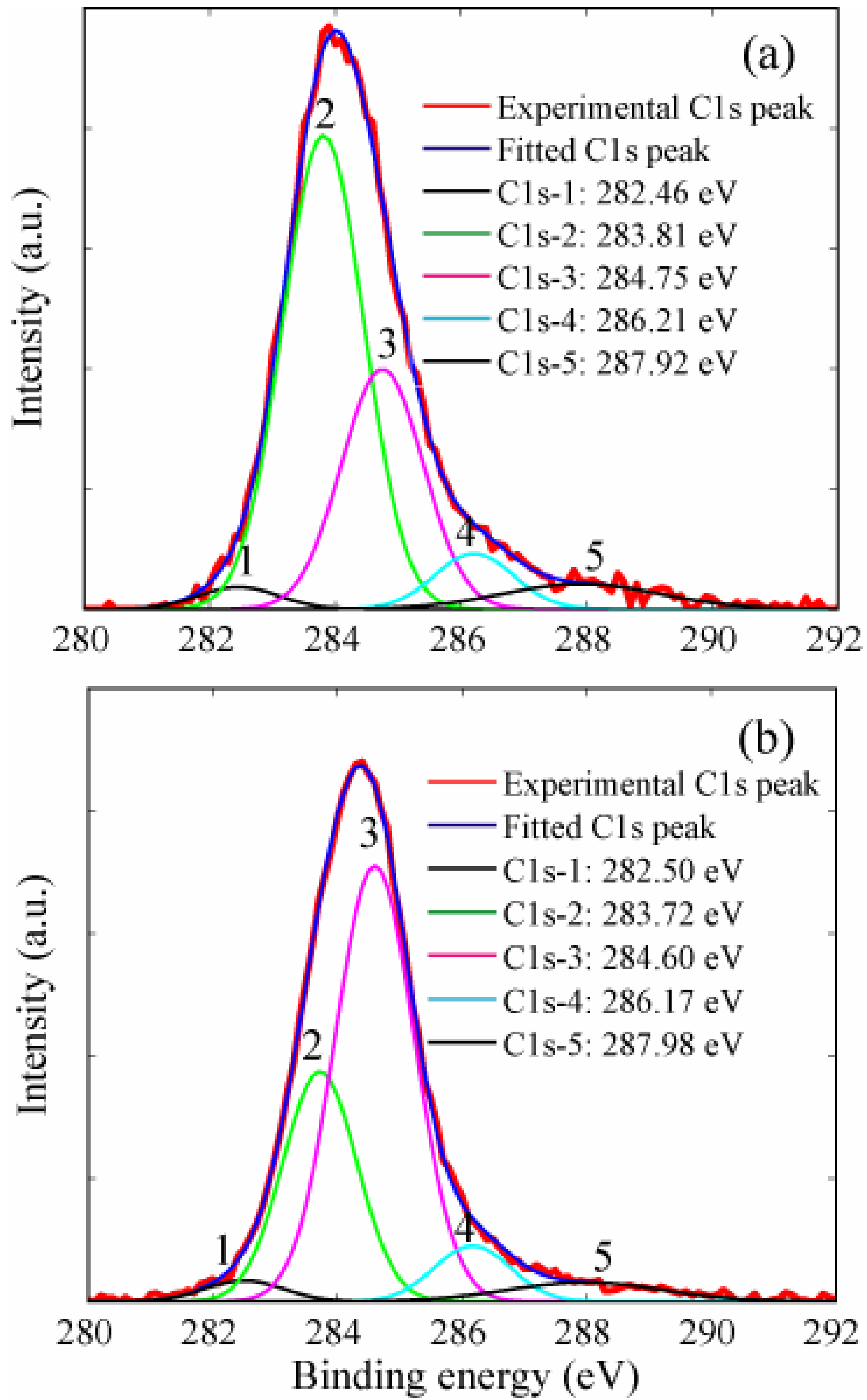

Figure 6

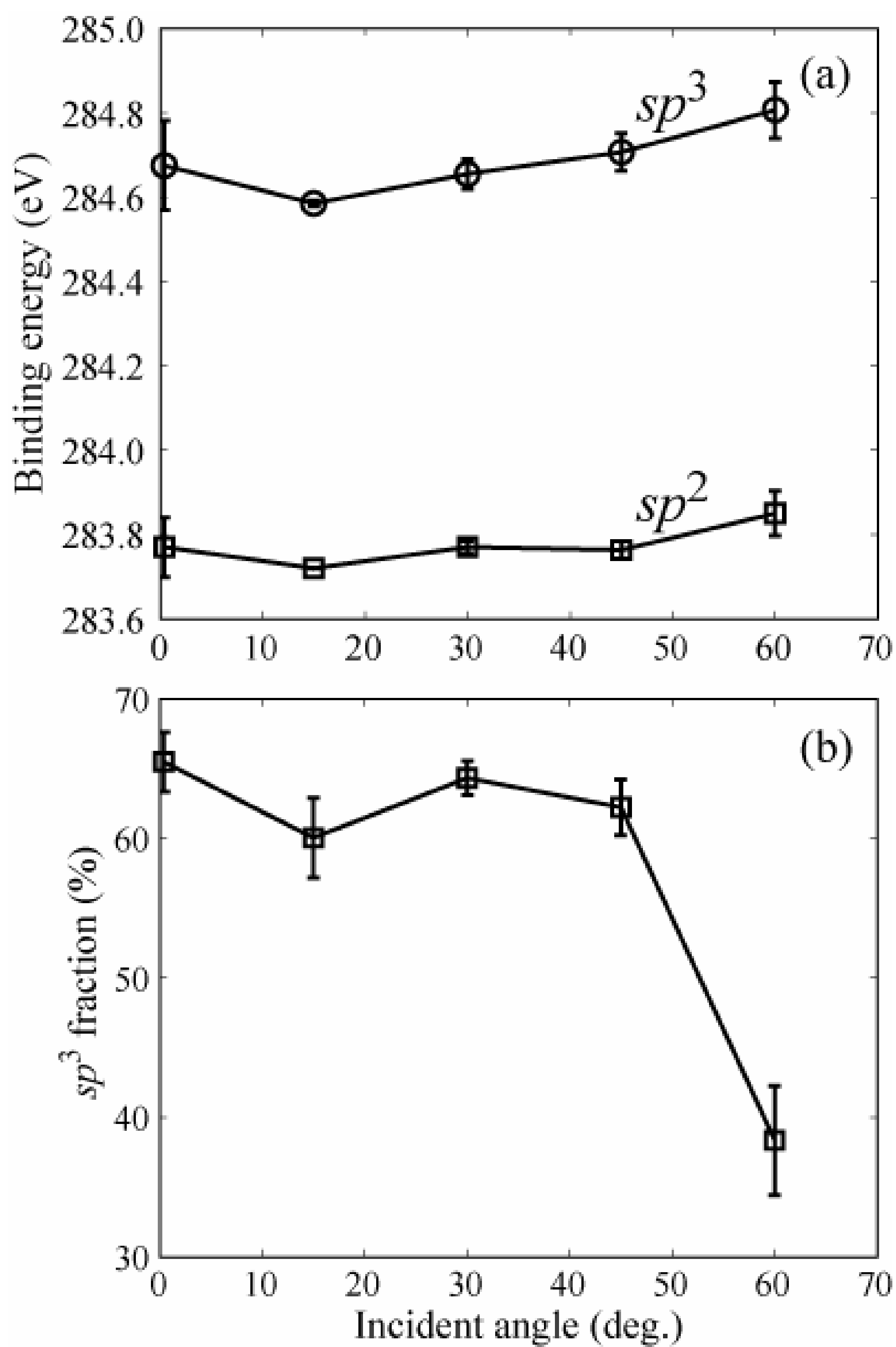

285.0
284.8
284.6
284.4
284.2
284.0
283.8
283.6
Binding energy (eV)
(a)
sp3
sp2
0
10
20
30
40
50
60
70
70
60
50
40
30
sp3 fraction (%)
(b)
Incident angle (deg.)

Figure 7

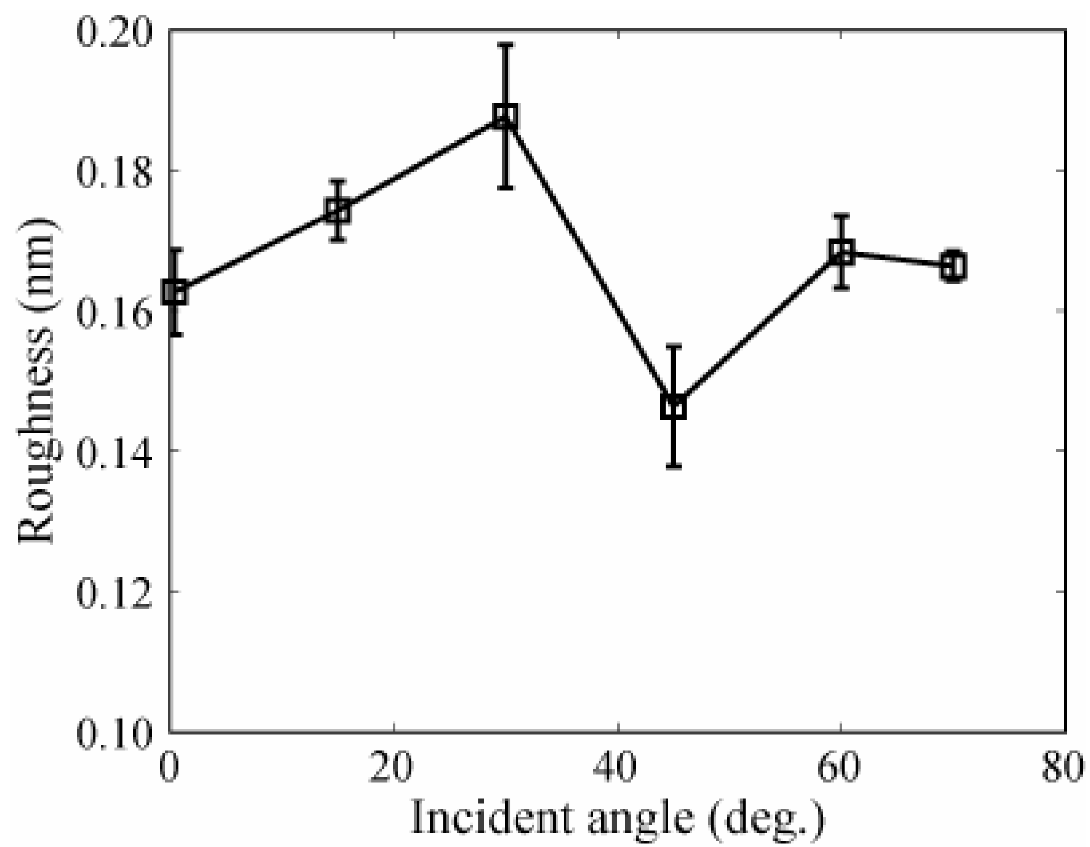

Figure 8

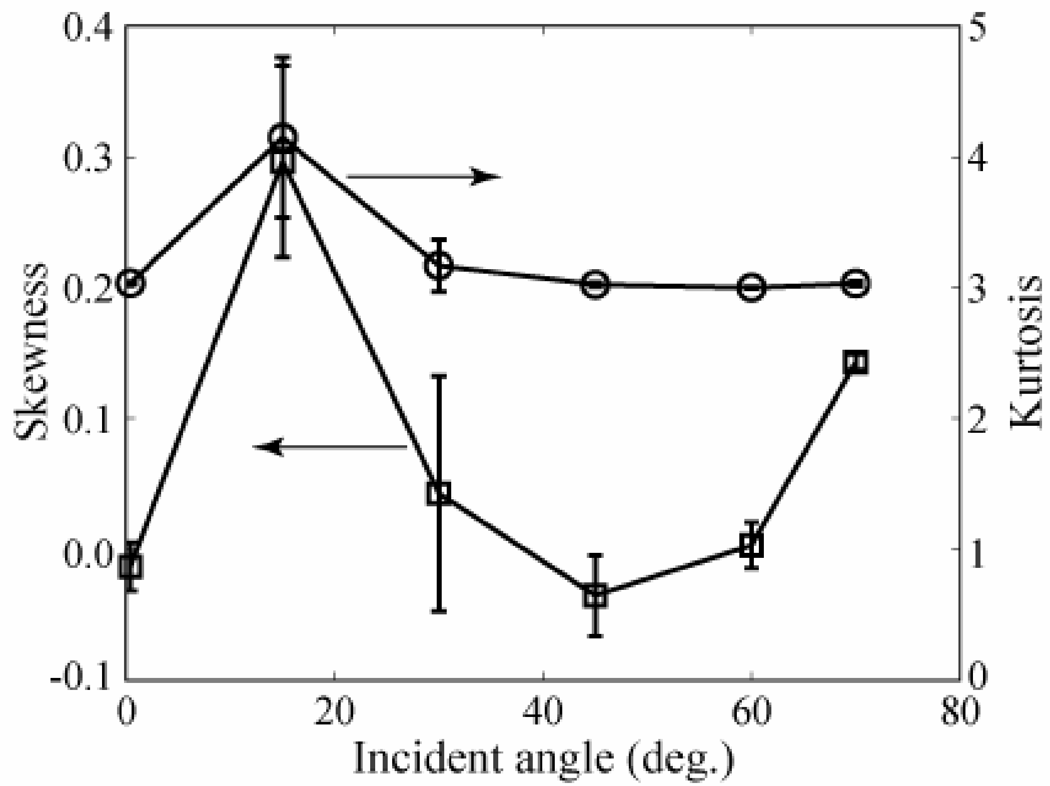

Figure 9